Int J Adv Manuf Technol (2018) 94:2729–2737
DOI 10.1007/s00170-017-1100-9

ORIGINAL ARTICLE

A comparative study on the modelling of EDM and hybrid electrical discharge and arc machining considering latent heat and temperature-dependent properties of Inconel 718

Afzaal Ahmed[1] · **A. Fardin**[1] · **M. Tanjilul**[1] · **Y.S. Wong**[1] · **M. Rahman**[1] · **A. Senthil Kumar**[1]

Received: 3 May 2017 / Accepted: 12 September 2017 / Published online: 18 September 2017

Abstract Inconel 718 is one of the most widely used super alloys in industries like oil and gas, aerospace and automobile. However, properties like poor thermal conductivity and work hardening tendency make it difficult to machine, using a conventional machining approach. EDM is one of the effective and efficient ways of machining this exotic material. However, the material removal rate (MRR) is very low. In an attempt to enhance the performance of EDM, an arc machining module has been integrated into the existing EDM system and the compound process is named hybrid electrical discharge and arc machining (HEDAM). Due to the high thermal intensity of the sparks/arcs imparted by this process, the material removal rate is elevated.

To understand this process better, a comparative thermal modelling between HEDAM and EDM has been presented in this article. Firstly, a thermal analysis is performed for the EDM and HEDAM processes to understand their respective erosion efficiencies. Finally, the numerical simulation for MRR of both EDM and HEDAM is presented. Unlike other EDM models, in this simulation, the thermophysical properties of the material were considered to be temperature-dependent and the latent heat of fusion was incorporated into the modelling process. A comparative analysis was also performed, which showed that incorporating such variables increases the accuracy of the obtained results. The study revealed that the spark radius in HEDAM is larger in size and more stable. Consequently, this resulted in HEDAM to have about three times more erosion efficiency compared to conventional EDM.

Keywords EDM · Hybrid machining · Simulation · Erosion efficiency · Spark radius

1 Introduction

Inconel 718, a nickel-based alloy with superior strength and thermal-resistant properties, is often used in the aerospace and the oil and gas industries. It is one of the most difficult materials to machine conventionally, being associated with shorter tool life and severe metallurgical damage to the workpiece [1]. This is mainly due to its work-hardening effects, which causes the cutting forces to rise progressively as the machining process prolongs. In addition, its poor thermal conductivity leads most of the heat generated to dissipate onto the cutting tool, which further accelerates the wear of the tool material [2]. All these contribute to a short tool life [3].

To avoid the drawbacks of conventional machining, non-contact machining processes like EDM is more frequently being used for the machining of Inconel 718 [4]. EDM removes material through spark erosion, with negligible cutting force. However, the material removal rate (MRR) associated with EDM is still very low compared to other mechanical machining processes. Due to this fact, the conventional EDM process is not able to fulfil the increasing demands of today's fast-moving manufacturing industry. To resolve this issue, a Hybrid Electrical Discharge and Arc Machining (HEDAM) process has been developed, which is a combination of EDM and arc machining process. Since HEDAM is a new process, its material removal mechanism is not entirely comprehensible. Fortunately, HEDAM is a thermal machining process like the EDM and EDM models are usually described

✉ Afzaal Ahmed
mpeafa@nus.edu.sg; afzaalahmed86@gmail.com

[1] Department of Mechanical Engineering, National University of Singapore (NUS), 9 Engineering Drive 1, Singapore 117576, Singapore

based on the thermomechanical process. Thus, the basic principles of EDM modelling can be considered for HEDAM modelling as well. However, most of the EDM models, including that by Somashekhar et al. [5], Yadav et al. [6] and Allen et al. [7], considered the thermophysical properties for the workpiece to be invariant and ignored the latent heat of fusion. Others, like Tilili et al. [8], considered the effects of temperature-dependent material properties but disregarded the impact of the latent heat of fusion. In reality, the thermophysical properties of materials vary with temperature. This, along with the latent heat of fusion, can affect the simulation results greatly.

Based on the abovementioned issues, an attempt has been made in this paper to model the MRR of EDM and HEDAM, by considering temperature-dependent material properties and the latent heat of fusion. Firstly, a thermal analysis is proposed for the EDM and the HEDAM processes, based on the Calorimetry equations, to understand their respective erosion efficiencies. Finally, the numerical simulations of the EDM and the HEDAM processes are presented to understand the difference in spark radius size in these two processes. Furthermore, to validate the statement that the temperature dependence of the material properties influence the accuracy of the model, a comparative simulation analysis was also performed with different combinations of temperature-dependent material properties and latent heat of fusion variable. For the numerical analysis, the thermal analysis features of the commercially available software, ANSYS APDL, were used. The results showed a significant improvement in the accuracies of these models.

2 Experimental setup

2.1 Machine tool

The experiments were performed on a especially developed multipurpose machine tool work table size of 250 mm × 350 mm and an axis travel capability of (*X*, *Y*, *Z*) 200 mm × 300 mm × 300 mm. In addition, the machine tool has an electrode guiding arrangement to minimise the wobbling of electrode during operation. The study uses the experimental setup shown in Fig. 1.

2.2 Workpiece and electrode material composition and machining parameters

The workpiece and tool materials selected for the study is Inconel 718 and copper tungsten (CuW) respectively. The properties of the workpiece and electrode materials are given in Table 1, while the machining parameters for the experiments are displayed in Table 2.

2.3 Working principle

The working principle of the circuit is illustrated in Fig. 2. A simple circuit diagram occupies the part (a) of the figure. The diodes ensure that current from the DC supply does not flow into the pulsed power supply and vice versa. Initially, the process begins with conventional EDM, where machining takes place during the t_{on} (on time) and ceases during the t_{off}

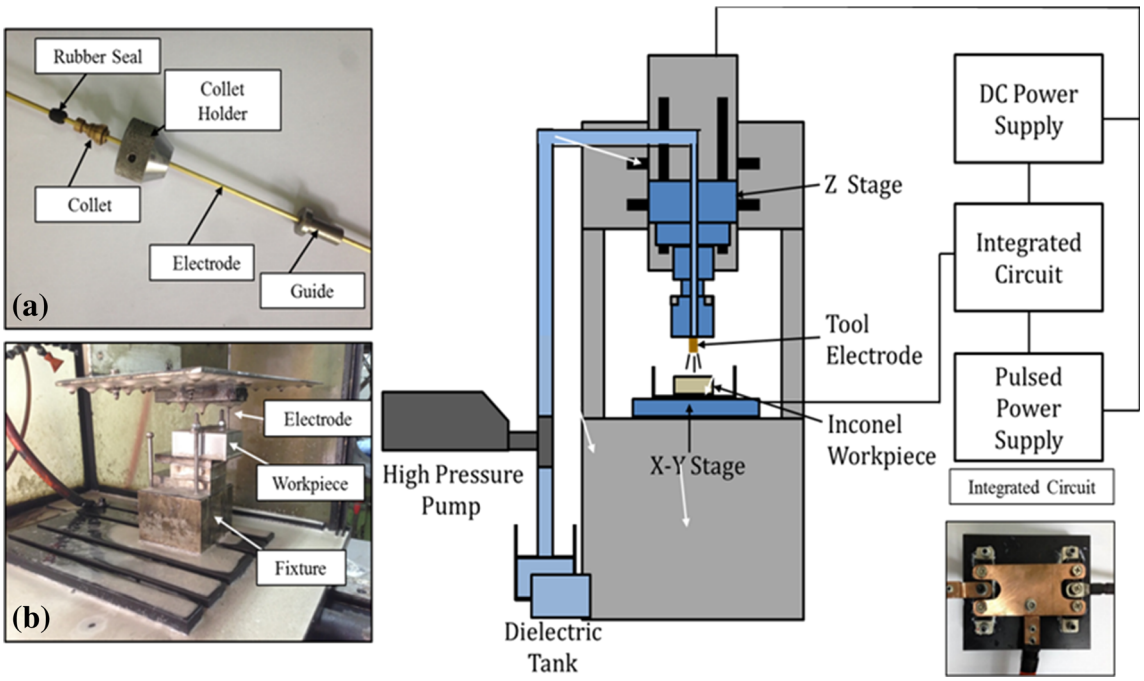

Fig. 1 Experimental setup for HEDAM (a) Collet-Electrode-Guide arrangement (b) Tool electrode and workpiece arrangement

Table 1 Composition of workpiece material and tool electrode

Workpiece material	Inconel 718
Composition (wt.%)	51% Ni; 20% Fe 18% Cr; 6% Nb; 4% Mo; 1% Ti
Tool material	Copper, Tungsten
Composition (wt.%)	25% Cu; 75% W

(off time). Subsequently, when the DC power supply is turned on, an additional current is supplied to the system.

Ideally, in reference to the circuit in Fig. 2a, an equalised voltage arrangement, assuming ideal diodes, will cause the current from each of the power sources to add. However, in reality, a voltage drop will be experienced across the diodes, which may not always cause the desired addition of current. In this paper, the diodes were considered to be ideal, and hence, the current output was its direct consequence.

The voltages of the constant DC power supply (V_{DC}) and the pulsed power supply (V_{PDC}) were equalised ($V_{DC} = V_{PDC}$). This will ensure that both the diodes (D1 and D2) in the circuit are in forward biased condition. Hence, during the t_{on}, the current from the pulsed power supply (I_{PDC}) adds to the current from the DC power supply (I_{DC}), causing the electric arc to appear in the plasma channel. However, during t_{off}, D2 gets reversed biased causing no current to flow through it. Hence, the system draws current only through D1 from DC power supply. The current profile of HEDAM is shown in part (b) of Fig. 2.

In HEDAM, the high current density generates high temperature and pressure inside the plasma channel, which melts the workpiece material rapidly. In addition, the high-pressure flushing and high rotational speed of the electrode aid to break the plasma channel continuously through deionisation, resulting in the cycle to begin anew.

Table 2 Machining parameters of HEDAM

Parameters	HEDAM	Unit
Current from the DC power supply (I_{DC})	50, 80, 110, 140	A
Current from the pulsed power supply (I_{PDC})	35	A
Voltage of DC power supply (V_{DC})	60	V
Peak voltage of pulsed power supply (V_{PDC})	60	V
Pulse on time of pulsed power supply (t_{on})	20	μs
Pulse off time of pulsed power supply (t_{off})	20	μs
Flushing pressure	8	MPa
Rotational speed	2000	rpm
Workpiece polarity	Positive	–

3 Thermophysical properties of workpiece materials

The thermophysical properties of a material like melting temperature (T_m), thermal conductivity, specific heat capacity (C_p) and latent heat of fusion (L_f) play a decisive role in the thermal machining process by influencing its machinability. However, it is difficult to find temperature-dependent data for different materials over a wide range of temperatures, especially in the case of alloys. Thus, the temperature-dependent material properties used in the modelling were compiled from multiple sources. For example, the thermal conductivity data as shown in Fig. 3 was acquired from the works of Sweet et al. [9] and Ahn et al. [10]. On the other hand, the specific heat data, as shown in Fig. 4, was collected from the Ahn et al. [10], Basak et al. [11] and Brooks et al. [12].

Another important material property is the latent heat of fusion (L_f), which is defined as the amount of thermal energy (Q) absorbed during the phase change from solid to liquid of 1 kg of the material. The consumption of the latent heat takes places over a certain range of temperature: usually referred to as the solidus-liquidus zone. For Inconel 718, the L_f is 227,000 J/kg and this energy is distributed to the system within solidus (1528 K) to liquidus (1610 K) temperature zone [13]. Since it is distributed over a range, it can be considered as a secondary specific heat, henceforth referred to as the specific latent heat capacity and it is the amount of energy required for phase change per unit temperature in the solidus-liquidus zone. Figure 4 shows both the specific heat capacity and the specific latent heat capacity. The summation of these two (specific heat capacity and specific latent heat capacity) is the apparent specific heat capacity and this merged entity has been used in the simulations to account for the latent heat of fusion.

4 Thermal analysis model

Erosion efficiency of a thermal process is defined as the percentage of input energy that ultimately goes towards the erosion of the material. Singh et al. [14] and Wong et al. [15] showed that the erosion efficiency of EDM is usually a very small percentage of the total amount of supplied energy. On the other hand, HEDAM is associated with even higher discharge energy in the machining gap compared to conventional EDM. Hence, to evaluate the erosion efficiencies of EDM and HEDAM, thermal energy analyses have been carried out. In both the cases, an erosion efficiency parameter was used and the energy equation was considered up to the melting point (the higher bound of the solidus-liquidus zone) of Inconel 718 (1610 K), as the erosion mechanism in EDM is mostly due to the phenomenon of melt-splashing at high energy [15].

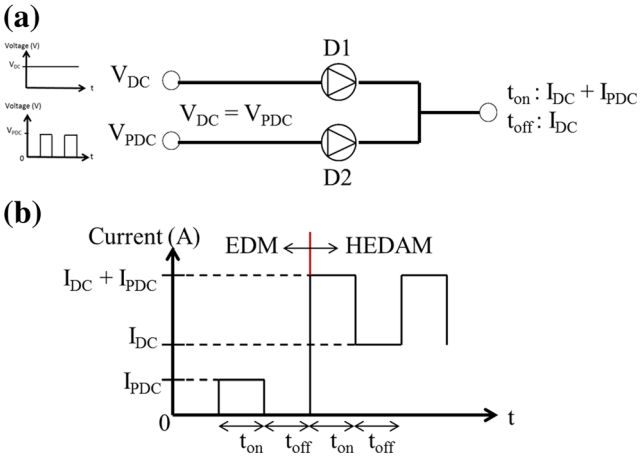

Figure 2 Schematic circuit (**a**) and output current profile (**b**) for HEDAM

- Energy supplied for erosion through an EDM process =

$$E_{\mathrm{EDM}} \times t_{\mathrm{m}} \times \left(\frac{t_{\mathrm{on}}}{t_{\mathrm{on}} + t_{\mathrm{off}}} \times V_{\mathrm{PDC}} \times I_{\mathrm{PDC}} \right) \quad (1)$$

- Energy supplied for erosion through a HEDAM process =

$$E_{HEDAM} \times t_{\mathrm{m}} \times \left\{ (V_{\mathrm{DC}} \times I_{\mathrm{DC}}) + \left(\frac{t_{\mathrm{on}}}{t_{\mathrm{on}} + t_{\mathrm{off}}} \times V_{\mathrm{PDC}} \times I_{\mathrm{PDC}} \right) \right\} \quad (2)$$

As the energy equation was considered from the room temperature to the melting point of the material,

$$Energy\ required\ \text{for}\ erosion = m \left(\int_{T_0}^{T_{\mathrm{m}}} C_{\mathrm{p}} \mathrm{dT} + L_{\mathrm{f}} \right) \quad (3)$$

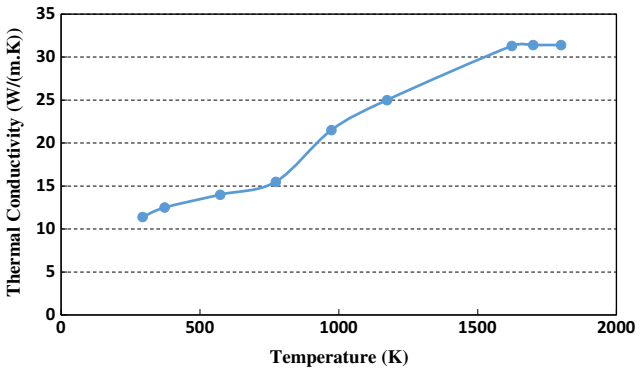

Fig. 3 Compilation of data for the thermal conductivity of Inconel 718 with temperature [9, 10]

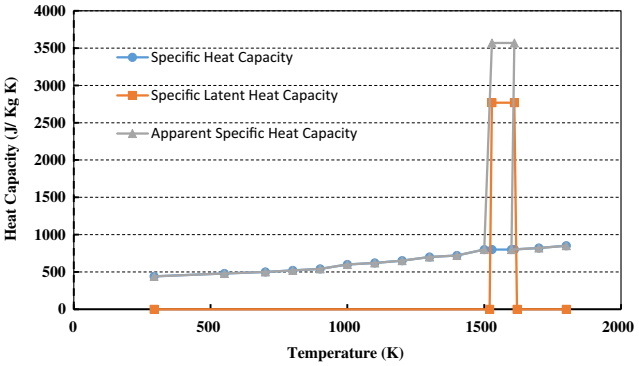

Fig. 4 Compilation of data for the heat capacity of Inconel 718 with temperature [10–12]

where E_{EDM} is the erosion efficiency of EDM, E_{HEDAM} is the erosion efficiency of HEDAM, t_{m} is the machining time, m is the mass eroded, T_{m} is the melting temperature of Inconel 718, T_0 is the room temperature, L_{f} is the latent heat of fusion and C_{p} is the specific heat capacity.

Since the supplied energy is equal to the energy received, Eqs. (1) and (3) can be equated for the EDM to solve for E_{EDM}. Similarly, Eqs. (2) and (3) can be equated to solve for E_{HEDAM}.

5 Numerical analysis model

EDM is a repetitive and randomly distributed spark machining process where electric spark occurs in the gap between the electrode and workpiece. In HEDAM, there is a continuous flow of current. However, there is a variation in the amplitude of the total current, as can be seen in Fig. 2, which makes the process more complex. To understand the HEDAM process better, a numerical simulation based model has been developed. In addition, the effect of temperature-dependent thermophysical properties of the workpiece and the latent heat of fusion has been considered in this proposed model. The following assumptions are made to make the problem mathematically feasible:

- As there was a variation of current in HEDAM due to its pulsed current profile, the process is modelled with multiple load steps.
- Thermal properties of workpiece material are functions of temperature and the analysis is considered as transient.
- The density and shape of the mesh elements are not affected by the thermal expansion.
- The workpiece material is isotropic and homogenous.
- Heat transfer to electrode surface is dissipated only by conduction.
- Radiation and convective heat losses are negligible.

- The heat flux of the both EDM and HEDAM behave as an ideal Gaussian distribution.
- The ambient temperature is room temperature (298 K).

5.1 Governing equations

Discharge phenomenon in both EDM and HEDAM are modelled by considering the heating of the workpiece by an incident heat flux. Fourier heat conduction equation which is applicable for the transient and non-linear thermal analysis has also been considered. The differential equation governing the heat conduction in an axisymmetrical solid surface is given by [16]:

$$\rho Cp\frac{dT}{dt}=\frac{1}{r}\frac{d}{dr}\left(Kr\frac{dT}{dr}\right)+\frac{d}{dz}\left(K\frac{dT}{dz}\right) \tag{4}$$

where ρ is the density, C_p is the specific heat, K is the thermal conductivity of the work material, T is the temperature, t is the time, and r and z are coordinate axes.

Kansal et al. [17] have shown that Eq. (4) can be re-written in a matrix form as follows:

$$[C_g]\{\dot{T}_G\}+[K_G]\ \{T_G\}=\{\dot{Q}_G\} \tag{5}$$

where C_g = global capacitance (specific heat) matrix, $[K_G]$ = global conductivity matrix, $\{\dot{Q}_G\}$ = global heat flux vector, $\{T_G\}$ = global temperature vector, and $\{\dot{T_G}\}$ = time derivative of $\{T_G\}$.

Commercially available numerical simulation solver ANSYS Mechanical APDL has been used to solve Eq. (5).

5.2 Heat flux model

Many researchers, including Yadav et al. [6], Weingärtner et al. [18] and Patel et al. [19], have reported that for the thermal machining processes like EDM, the heat flux can be closely approximated by a Gaussian function, as illustrated in Fig. 5. Furthermore, this model has also been applied for the heat flux in the striking arc machining process [20] and even for arc welding process [21].

Gaussian curve model within a deviation of − 3σ to + 3σ region can be expressed as follows for a random variable r: [18]

$$Q(r)=\frac{3}{\sqrt{2\Pi}R}e^{-4.5\frac{r^2}{R^2}} \tag{6}$$

where $Q(r)$ is used to express the intensity of heat imparted to the workpiece.

For EDM and HEDAM, at $r=0$, $Q(r)=Q_0$; where Q_0 is the maximum heat intensity.

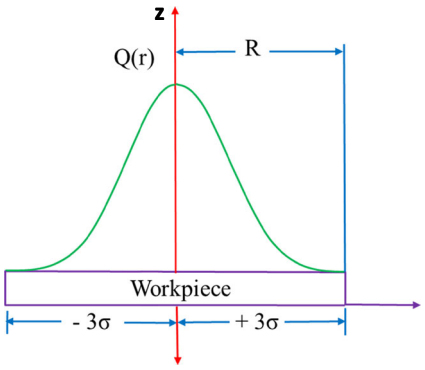

Fig. 5 Gaussian heat distribution of the heat source

Hence, Eq. (6) can be written as:

$$Q(r)=Q_0\ e^{\left(-4.5r^2/R^2\right)} \tag{7}$$

For a circular area, the heat flux in Eq. (7) could be integrated as follows to find incident energy on the workpiece:

$$E=\int Q(r)dA=\int_0^R Q(r)2\pi rdr=0.2191\pi Q_0R^2d \tag{8}$$

Since the energy supplied is equal to energy received, Eq. (8) can be equated to the energy supplied per unit time for EDM and HEDAM, which is:

$$E=\eta VI \tag{9}$$

where η is the fraction of heat input that is imparted to the workpiece and R is the spark radius. The parameter η should not be confused with E_{EDM} or E_{HEDAM}, which are the erosion efficiency parameters. V and I represent the voltage and the current at the respective load step, which contribute to the input energy.

Therefore,

$$\begin{aligned}&\eta VI=0.2191\pi Q_0R^2\\&or,\ Q_0=\frac{4.5\eta VI}{\pi R^2}\end{aligned} \tag{10}$$

By substituting Eq. 10 in Eq. 7, Eq. 11 can be obtained:

$$Q(r)=\frac{4.5\eta VI}{\pi R^2}e^{-4.5\frac{r^2}{R^2}} \tag{11}$$

This has been used as heat flux function in these analyses.

In HEDAM, an η value of 0.25 can be considered as proposed by Zhang et al. [22]. For EDM, varying η values that changes with current was considered as proposed by Singh and Shukla [14].

5.3 Spark radius model

An empirical formula was modelled for EDM and HEDAM spark radius. Little data was available regarding arc diameter in the existing literature. Recently, Zhang et al. [22] mentioned that the diameter of the arc burning in the air freely can be described based on the following formula:

$$D = 260 \times I^{0.5}(\mu m)$$

where D is the diameter of the arc, in micrometres and I is the discharge current, in amperes.

Many researchers, including Erden [23] and Shabgard et al. [24], have proposed an EDM spark radius model, where the spark radius is dependent not only upon current (I) but also upon the pulse on time (t_{on}) and the voltage (V). Since all the EDM experiments in this paper were conducted at a fixed t_{on} and V, the EDM spark radius formula was simplified with just current (I) as the independent variable.

Thus, for both EDM and HEDAM only current was considered for the empirical spark radius formula, which is shown below:

$$R = k \times I^{n}(\mu m) \tag{12}$$

where k and n are constants. The values of k and n depend on the various influencing parameters that affect EDM and HEDAM, which includes flushing pressure, voltage and the rotational speed of electrode. The k and n values were modelled for both the processes in the numerical simulation and the following spark radius formulae were obtained.

$$R_{HEDAM} = 4.5 \times I^{0.44}(\mu m) \tag{13}$$

$$R_{EDM} = 1.3 \times I^{0.77}(\mu m) \tag{14}$$

5.4 Modelling in ANSYS

A 2D axisymmetric model was considered around the z-axis for both the processes. Therefore, the thickness of the material was not taken into consideration.

Appropriate boundary conditions as shown in Fig. 6 were selected. Heat flux for each spark was applied on the surface B, up to the spark radius R using Gaussian distribution. Since the boundaries C and D are far from spark radius and the spark has been made to strike for a short duration, no heat transfer condition was considered for them. Furthermore, no heat transfer condition was also considered for boundary A as it is the axis of the symmetry.

Summary of the boundary conditions is provided below:

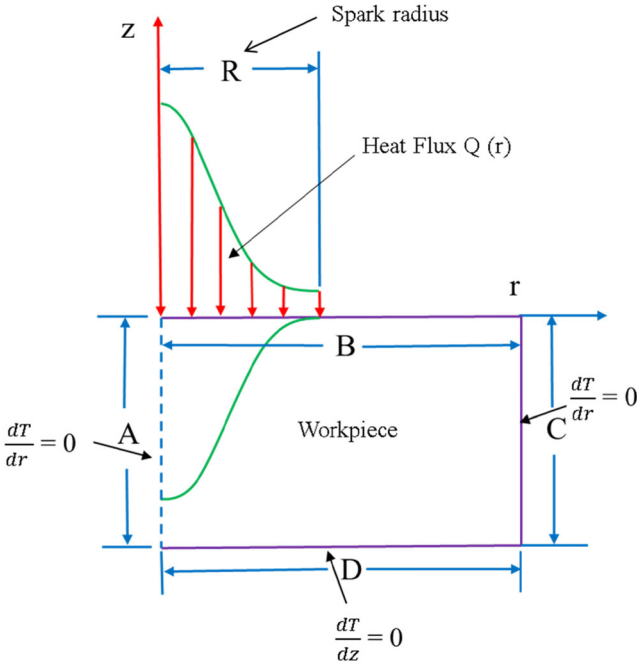

Fig. 6 Heat transfer model of the thermal system

6 For boundary B

Up to spark radius, R:

$$K\frac{dT}{dz} = Q(r)$$

7 For boundaries A, C and D

$$\frac{dT}{dz} = 0 \; and \; \frac{dT}{dr} = 0$$

In ANSYS, a work geometry was constructed by using mapped meshing technique for transient thermal analysis, and "Quad 4node 55" was chosen as the element type. In every 20 μs, there is a variation in load current in HEDAM. Hence, the simulation was conducted for 40 μs with two different load steps. In the case of EDM, there is also a variation of current in every 20 μs. However, since the current is zero in one of the load steps (during t_{off} in EDM), only t_{on} load step is responsible for the erosion. Thus, only one load step was considered for EDM. After the simulation was conducted in ANSYS, a temperature distribution plot of the workpiece was produced for both the processes. The elements with a temperature above 1610 K (melting temperature of Inconel 718) were killed off, leaving a crater like the one shown in Fig. 7 below.

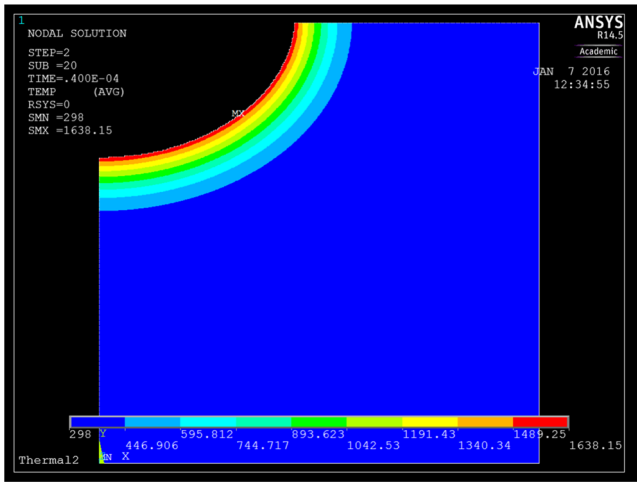

Fig. 7 ANSYS-simulated crater for HEDAM with temperature distribution

Crater volume was measured considering it as a part of a sphere, and then MRR per minute was calculated based on the frequency of discharges.

7.1 Removal efficiency

Since EDM is a discontinuous process, the plasma channel collapses during the t_{off} time, causing a momentary stop in the melting process. However, the dielectric fluid continues to flow. Thus, a large proportion of the material molten during the t_{on} time cools down and re-solidifies. Pandey and Jilani have shown that only about 20% of the molten material is effectively removed and contributes to the MRR during EDM [25]. This parameter is termed as the removal efficiency. On the other hand, HEDAM is a continuous process, where the plasma channel continues to be maintained even during the t_{off} time of the EDM. Thus, it is assumed that little or no re-solidification occurs. Hence, the removal efficiency term for HEDAM was considered 100% for simplification. This removal efficiency term should not be confused with the parameters η or E_{EDM}/E_{HEDAM}.

8 6. Result and discussion

8.1 Thermal analysis

From Eq. (1) in Section 4, it has been found that at different current settings and 20-μs pulse duration, the erosion efficiency for EDM (E_{EDM}) corresponds to a value of 0.2%. This value is slightly higher than the erosion efficiencies proposed by Singh et al. [14] and Wong et al. [15]. Figure 8 illustrates a comparison between the experimental MRR of EDM and the theoretical MRR using the calculated E_{EDM}. Using Eq. (2) for HEDAM, the thermal analysis was carried out for different

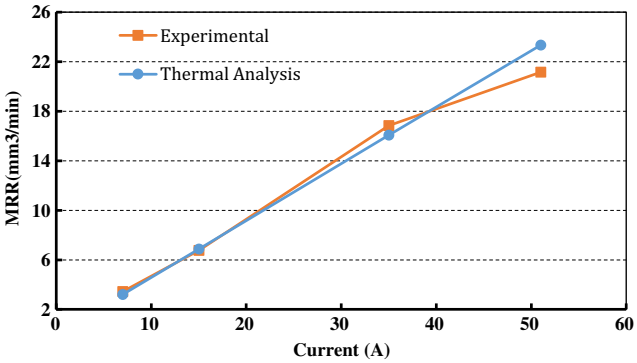

Fig. 8 Experimental versus thermal analysis MRR for EDM

current settings of DC power supply, keeping the value of current from the pulse power supply constant at 35 A. It has been found that at 0.55% erosion efficiency (E_{HEDAM}), the thermal analysis MRR values show good correlation with the experimental results. This can be observed in Fig. 9.

The comparison of the thermal models for EDM and HEDAM shows that HEDAM has a better erosion efficiency than that of EDM. In the case of EDM, the discharge is not continuous due to the pulsating nature of the power supply. Thus, a spark appears at a time interval of t_{on}, followed by no spark during t_{off}. On the contrary, in HEDAM, a stable arc is formed due to the continuous current from the DC power supply which leads to continuous machining and higher erosion efficiency.

Additionally, Fig. 9 also shows that, for HEDAM at 50 A current setting, the experimental MRR value is slightly higher than the theoretical thermal analysis value. This indicates that HEDAM is more efficient at lower current settings. However, the efficiency at higher current settings can also be improved through optimisation of flushing, control systems and the electrode design.

8.2 Numerical analysis

Four different approaches have been carried in the HEDAM simulation process to validate the feasibility of the developed

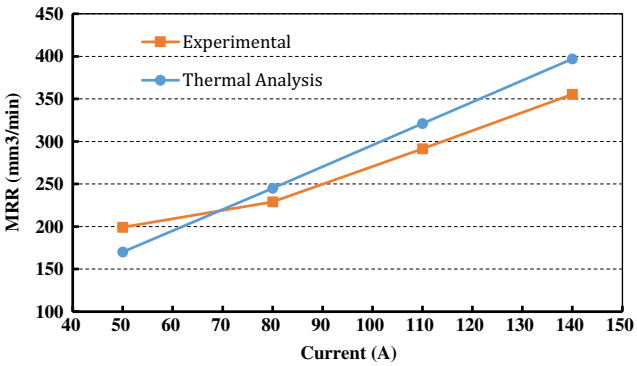

Fig. 9 Experimental versus thermal analysis MRR for HEDAM (varying constant DC current with 35 (A) constant pulse current)

material removal model. In the first approach, all the thermal properties of the material were considered constant with respect to temperature and the latent heat of fusion was ignored. Although it is the most common approach, it does not corroborate with the experimental values in Fig. 10 at all.

In the second simulation, specific heat was considered to be temperature-dependent, while the other thermal properties of the material remained invariant; the latent heat of fusion was also ignored. Here, the difference with the experimental MRR values is lower than the previous case. From Fig. 4, the specific heat increases when the temperature is increased. Thus, the ability of the material to store thermal energy increases. The thermal energy tends to stay more concentrated instead of being transmitted into the material. The reason for the deviation can be attributed to the fact that thermal conductivity has been constant with respect to temperature for this simulation.

In the third simulation, the specific heat of the workpiece was taken to be temperature-dependent, and the latent heat of fusion was also taken into consideration. A significant amount of energy is involved in the change of phases and it cannot be ignored. If ignored, the rise of temperature after the solidus point becomes faster, causing an increase in the amount of molten material. In this case, simulation results showed a better trend with the experimental results as compared to the previous cases.

In the final HEDAM simulation, all the thermophysical properties of the workpiece were assumed to be temperature-dependent, and the latent heat of fusion was taken into consideration. In this case, the simulation results correlated well with the experimental results. A possible reason for the slight difference is due to the lack of temperature-dependent data above the solidus point (1520 K) for Inconel 718.

Moreover, to compare the spark radius size of HEDAM with EDM, an EDM simulation was conducted by considering temperature-dependent materials properties and the latent heat of fusion. This correlated well with experimental results. This can be observed in Fig. 11.

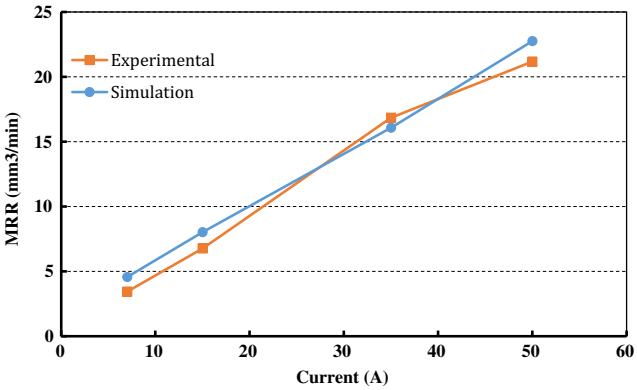

Fig. 11 Experimental versus simulation MRR result for EDM of Inconel 718

From Eqs. (13) and (14), it has been identified that in HEDAM, the spark radius is significantly higher than that of EDM. This is because, in EDM, a spark disappears rapidly and another spark discharge appears soon after. On the contrary, in the HEDAM, a stable arc is generated due to the continuous DC power supply attached to the EDM pulse power supply. This results in a larger and stable plasma channel which influences the erosion efficiency.

9 Conclusions

In this paper, a thermal and numerical analysis modelling has been carried out for EDM and HEDAM considering temperature-dependent material properties and the latent heat of fusion of Inconel 718. Following conclusions can be drawn from the analysis:

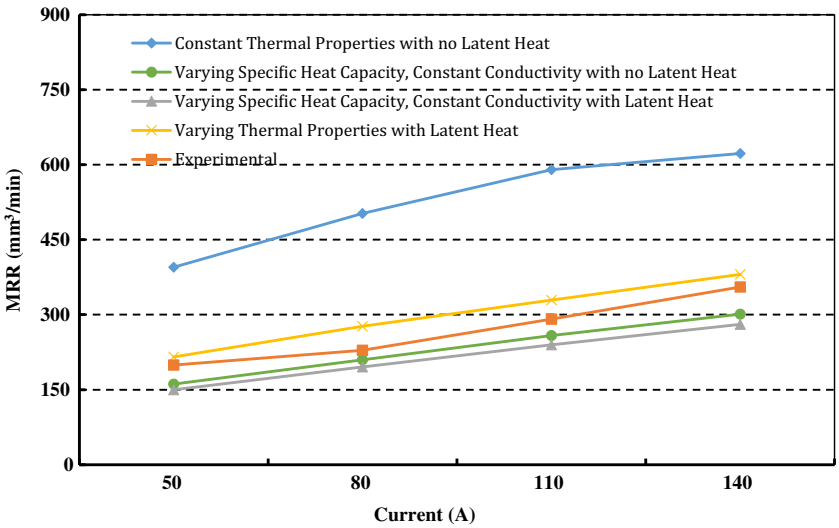

Fig. 10 Experimental versus various simulation MRR result for HEDAM of Inconel 718

- A thermal and numerical model has been successfully developed to evaluate the MRR of EDM and HEDAM.
- From the thermal analysis, it has been found that the HEDAM has higher erosion efficiency compared to EDM.
- The simulation results correlated well with the experimental results when the temperature-dependent material properties and the latent heat of fusion were considered.
- From spark radius analysis, it has been identified that due to the stability and bigger size of the spark radius in HEDAM, it is comparatively more energy efficient (higher erosion efficiency).

Acknowledgements The authors would like to thank Dr. S. Panda and Mr. J. Adhikari for their contributions. This work was funded by A*Star (Grant No: R265-000-534-305) and Singapore Institute of Manufacturing Technology (SIMTech) (Grant No: R265-000-518-504).

References

1. Rahman M, Seah WKH, Teo TT (1997) The machinability of inconel 718. Journal of Materials Processing Tech 63(1):199–204. https://doi.org/10.1016/S0924-0136(96)02624-6
2. Dudzinski D, Devillez A, Moufki A, Larrouquère D, Zerrouki V, Vigneau J (2004) A review of developments towards dry and high speed machining of inconel 718 alloy. Int J Mach Tools Manuf 44(4):439–456. https://doi.org/10.1016/S0890-6955(03)00159-7
3. Umbrello D (2013) Investigation of surface integrity in dry machining of inconel 718. Int J Adv Manuf Technol 69(9):2183–2190. https://doi.org/10.1007/s00170-013-5198-0
4. Ay M, Çaydaş U, Hasçalık A (2013). Optimization of micro-EDM drilling of inconel 718 superalloy. Int J Adv Manuf Technol, 66(5–8), 1015-1023
5. Somashekhar KP, Panda S, Mathew J, Ramachandran N (2015) Numerical simulation of micro-EDM model with multi-spark. Int J Adv Manuf Technol 76(1–4):83–90. https://doi.org/10.1007/s00170-013-5319-9
6. Yadav V, Jain VK, Dixit PM (2002) Thermal stresses due to electrical discharge machining. Int J Mach Tools Manuf 42(8):877–888. https://doi.org/10.1016/S0890-6955(02)00029-9
7. Allen P, Chen X (2007) Process simulation of micro electro-discharge machining on molybdenum. J Mater Process Tech 186(1):346–355. https://doi.org/10.1016/j.jmatprotec.2007.01.009
8. Tlili A, Ghanem F, Salah NB (2015) A contribution in EDM simulation field. Int J Adv Manuf Technol 79(5):921–935. https://doi.org/10.1007/s00170-015-6880-1
9. Sweet JN, Roth EP, Moss M (1987) Thermal conductivity of inconel 718 and 304 stainless steel. Int J Thermophys 8(5):593–606. https://doi.org/10.1007/BF00503645
10. Ahn DG, Byun KW, Kang MC (2010) Thermal characteristics in the cutting of Inconel 718 Superalloy using CW Nd: YAG laser. J Mater Sci Technol 26(4):362–366. https://doi.org/10.1016/S1005-0302(10)60059-X
11. Basak D, Overfelt RA, Wang D (2003) Measurement of specific heat capacity and electrical resistivity of industrial alloys using pulse heating techniques. Int J Thermophys 24(6):1721–1733. https://doi.org/10.1023/B:IJOT.0000004101.88449.86
12. Brooks CR, Cash M, Garcia A (1978) The heat capacity of inconel 718 from 313 to 1053 K. J Nucl Mater 78(2):419–421. https://doi.org/10.1016/0022-3115(78)90463-4
13. Kamnis S, Gu S, Zeoli N (2008) Mathematical modelling of inconel 718 particles in HVOF thermal spraying. Surf Coat Technol 202(12):2715–2724. https://doi.org/10.1016/j.surfcoat.2007.10.006
14. Singh H, Shukla DK (2012) Optimizing electric discharge machining parameters for tungsten-carbide utilizing thermo-mathematical modelling. Int J Therm Sci 59:161–175. https://doi.org/10.1016/j.ijthermalsci.2012.03.017
15. Wong YS, Rahman M, Lim HS, Han H, Ravi N (2003) Investigation of micro-EDM material removal characteristics using single RC-pulse discharges. J Mater Process Tech 140(1):303–307. https://doi.org/10.1016/S0924-0136(03)00771-4
16. Kumar DS (2009) Heat And Mass Transfer (Two Colour). S. K. Kataria & Sons
17. Kansal HK, Singh S, Kumar P (2008) Numerical simulation of powder mixed electric discharge machining (PMEDM) using finite element method. Math Comput Model 47(11):1217–1237. https://doi.org/10.1016/j.mcm.2007.05.016
18. Weingärtner E, Kuster F, Wegener K (2012) Modeling and simulation of electrical discharge machining. Procedia CIRP 2:74–78. https://doi.org/10.1016/j.procir.2012.05.043
19. Patel MR, Barrufet MA, Eubank PT, DiBitonto DD (1989) Theoretical models of the electrical discharge machining process. II. The anode erosion model. J Appl Phys 66(9):4104. https://doi.org/10.1063/1.343995
20. Zhang B, Tian X, Wang W, Tang X, Wang P (2014) Numerical and experimental investigations on micro-detonation of striking arc machining of alumina. Proc Inst Mech Eng B J Eng Manuf 228(6):918–930. https://doi.org/10.1177/0954405413509078
21. Tsai NS, Eagar TW (1985) Distribution of the heat and current fluxes in gas tungsten arcs. Metall Trans B 16(4):841–846. https://doi.org/10.1007/BF02667521
22. Zhang Q, Zhang M, Wang H, Liu G, Guo T (2015) Research on a single pulse discharge to discriminate EDM and EAM based on the plasma tunnel and crater geometry. J Mater Process Tech 219:248–256. https://doi.org/10.1016/j.jmatprotec.2014.12.016
23. Erden A (1983) Effect of materials on the mechanism of electric discharge machining (E.D.M.) J Eng Mater Technol 105(2):132. https://doi.org/10.1115/1.3225627
24. Shabgard M, Ahmadi R, Seyedzavvar M, Oliaei SNB (2013) Mathematical and numerical modeling of the effect of input-parameters on the flushing efficiency of plasma channel in EDM process. Int J Mach Tools Manuf 65:79–87. https://doi.org/10.1016/j.ijmachtools.2012.10.004
25. Pandey PC, Jilani ST (1986) Plasma channel growth and the resolidified layer in edm. Precis Eng 8(2):104–110. https://doi.org/10.1016/0141-6359(86)90093-0